


RESEARCH ARTICLE

Open Access



Inhaled nitric oxide preserves ventricular function during resuscitation using a percutaneous mechanical circulatory support device in a porcine cardiac arrest model: an echocardiographic myocardial work analysis

Christoph Nix^{1,2†}, Rashad Zayat^{3*†} , Andreas Ebeling¹, Andreas Goetzenich^{1,2}, Uma Chandrasekaran⁴, Rolf Rossaint¹, Nima Hatam^{3†} and Matthias Derwall^{1†}

Abstract

Background: Resuscitation using a percutaneous mechanical circulatory support device (iCPR) improves survival after cardiac arrest (CA). We hypothesized that the addition of inhaled nitric oxide (iNO) during iCPR might prove synergistic, leading to improved myocardial performance due to lowering of right ventricular (RV) afterload, left ventricular (LV) preload, and myocardial energetics. This study aimed to characterize the changes in LV and RV function and global myocardial work indices (GWI) following iCPR, both with and without iNO, using 2-D transesophageal echocardiography (TEE) and GWI evaluation as a novel non-invasive measurement.

Methods: In 10 pigs, iCPR was initiated following electrically-induced CA and 10 min of untreated ventricular fibrillation (VF). Pigs were randomized to either 20 ppm (20 ppm, n = 5) or 0 ppm (0 ppm, n = 5) of iNO in addition to therapeutic hypothermia for 5 h following ROSC. All animals received TEE at five pre-specified time-points and invasive hemodynamic monitoring.

Results: LV end-diastolic volume (LVEDV) increased significantly in both groups following CA. iCPR alone led to significant LV unloading at 5 h post-ROSC with LVEDV values reaching baseline values in both groups (20 ppm: 68.2 ± 2.7 vs. 70.8 ± 6.1 mL, $p = 0.486$; 0 ppm: 70.8 ± 1.3 vs. 72.3 ± 4.2 mL, $p = 0.813$, respectively). LV global longitudinal strain (GLS) increased in both groups following CA. LV-GLS recovered significantly better in the 20 ppm group at 5 h post-ROSC (20 ppm: -18 ± 3% vs. 0 ppm: -13 ± 2%, $p = 0.025$). LV-GWI decreased in both groups after CA with no difference between the groups. Within 0 ppm group, LV-GWI decreased significantly at 5 h post-ROSC compared to baseline (1,125 ± 214 vs. 1,835 ± 305 mmHg%, $p = 0.011$). RV-GWI was higher in the 20 ppm group at 3 h and 5 h post-ROSC (20 ppm: 189 ± 43 vs. 0 ppm: 108 ± 22 mmHg%, $p = 0.049$ and 20 ppm: 261 ± 54 vs. 0 ppm: 152 ± 42 mmHg%, $p = 0.041$). The blood flow calculated by the Impella controller following iCPR initiation correlated well with the

*Correspondence: rzayat@ukaachen.de

†Christoph Nix and Rashad Zayat: both authors contributed equally first

†Nima Hatam and Matthias Derwall: both authors contributed equally last

³ Department of Thoracic and Cardiovascular Surgery, Medical Faculty, RWTH University Hospital Aachen, RWTH Aachen University, 52074 Aachen, Germany

Full list of author information is available at the end of the article



© The Author(s) 2021. **Open Access** This article is licensed under a Creative Commons Attribution 4.0 International License, which permits use, sharing, adaptation, distribution and reproduction in any medium or format, as long as you give appropriate credit to the original author(s) and the source, provide a link to the Creative Commons licence, and indicate if changes were made. The images or other third party material in this article are included in the article's Creative Commons licence, unless indicated otherwise in a credit line to the material. If material is not included in the article's Creative Commons licence and your intended use is not permitted by statutory regulation or exceeds the permitted use, you will need to obtain permission directly from the copyright holder. To view a copy of this licence, visit <http://creativecommons.org/licenses/by/4.0/>. The Creative Commons Public Domain Dedication waiver (<http://creativecommons.org/publicdomain/zero/1.0/>) applies to the data made available in this article, unless otherwise stated in a credit line to the data.

pulsed-wave Doppler (PWD) derived pulmonary flow (PWD vs. controller: 1.8 ± 0.2 vs. 1.9 ± 0.2 L/min, $r = 0.85$, $p = 0.012$).

Conclusions: iCPR after CA provided sufficient unloading and preservation of the LV systolic function by improving LV-GWI recovery. The addition of iNO to iCPR enabled better preservation of the RV-function as determined by better RV-GWI. Additionally, Impella-derived flow provided an accurate measure of total flow during iCPR.

Keywords: Left ventricular assist device, Percutaneous mechanical circulatory support, Cardiac arrest, Cardiopulmonary resuscitation, Left ventricular unloading, Nitric oxide, Impella

Background

Cardiac arrest (CA) remains associated with high mortality and poor functional outcome. Despite the growing clinical use of mechanical circulatory support (MCS) for cardio-pulmonary resuscitation (CPR) after CA, the contribution towards a higher survival rate and the better functional outcome is yet to be demonstrated. An animal study showed a beneficial effect of the early use of a percutaneous mechanical circulatory support device, termed intravascular CPR (iCPR), on post-CPR survival [1]. An additional inhaled nitric oxide (iNO) application in an animal model resulted in improved trans-pulmonary blood flow and was associated with improved neurological outcomes [2]. We hypothesized that the synergistic effects of iNO during iCPR were a result of improved myocardial performance due to lowering of right ventricular (RV) afterload, left ventricular (LV) preload, and myocardial energetics. Previous studies have demonstrated a cardio-protective effect of ventricular unloading by percutaneous MCS through reduction in myocardial wall stress and myocardial work (MW) [3]. Recently, echocardiographic MW assessment has emerged as a non-invasive method to evaluate myocardial performance and gain more insights into myocardial energetics and mechanics, given the strong correlation with invasive pressure–volume (PV) measurements [4].

Thus, in the present study, we aimed to better understand the effect of iNO during iCPR on the myocardial performance and mechanics in a well-established large animal model of CA [1, 2]. The left (LV) and right ventricular (RV) function before, during, and after iCPR were analyzed using 2-D transesophageal echocardiography (TEE), deformation imaging, tissue Doppler (TDI) and non-invasive myocardial work measurement. In addition, trans-pulmonary flow (TPF) inferred by pulsed-wave Doppler (PWD) during iCPR was compared to the calculated pump flow derived from the Impella controller.

Methods

The experimental protocol was approved by the appropriate governmental institution (Landesamt für Natur, Umwelt und Verbraucherschutz NRW (LANUV),

Recklinghausen, Germany) and has been previously described [1, 2]. All animals received adequate care according to the precepts of the Helsinki declaration. Ten healthy female swine (Deutsche Landrasse, *Sus scrofa domestica*), approximately four months of age, and weighing 44 to 57 kg were used in this study. Animals were sourced from the Institute for Laboratory Animal Research, University Hospital RWTH Aachen, Aachen, Germany. All pigs had a clinical examination on arrival at the facility. Animals were housed in pens with a 12 h-day-night cycle and access to drinking water ad libitum. Twelve hours before the experiment, the pigs were set on nil per os except for drinking water access. The experimental procedures were carried out in accordance with the ARRIVE guidelines 2.0 (Animal Research: Reporting of In Vivo Experiments) [5].

Animal instrumentation

Figure 1 provides an overview of animal instrumentation and the experiment model. The pigs were weighed before the start of the experiment. General anesthesia was induced by intramuscular injection of 4 mg/kg azaperone (Stresnil, Janssen-Cilag GmbH, Neuss, Germany), followed by intravenous injection of 15 mg/kg sodium pentobarbital (Narcoren, Boehringer Ingelheim Vet-medica GmbH, Ingelheim am Rhein, Germany). Anesthesia was maintained by continuous intravenous sodium pentobarbital infusion at a rate of 4 mg/kg/h. The pigs were placed in a supine position, intubated orotracheally, and the legs were fixed in an extended position. Animals were ventilated with an inspired oxygen fraction of 0.3 (Servo Ventilator 300A; Siemens AG, Munich, Germany). Tidal volume was set to 10 ml/kg, and respiratory rate was adjusted to keep the end-tidal carbon dioxide partial pressure within a physiologic range (35 ± 4 mmHg). A continuous five lead electrocardiogram (ECG) and pulse oximetry were performed. Convective air heating was used to maintain body temperature at 38 ± 0.5 °C during preparation (Warm Touch 5200; Tyco Healthcare, Pleasanton, CA, USA).

Hemodynamic monitoring

Arterial blood pressure was obtained using a fluid-filled catheter (Vygon, Ecquen, France) placed into the left femoral artery. For pulmonary artery pressure and cardiac output measurements, a Swan-Ganz catheter (744HF75; Edwards Lifesciences, Irvine, CA, USA) was flow-directed into the pulmonary artery and connected to a cardiac output monitor (Vigilance; Edward Lifesciences). Impella flow was taken from the motor current based flow calculation on the AIC (Automated Impella Controller) as described in detail earlier [6].

Cardiac arrest model

As described previously [1, 2], cardiac arrest was induced using an alternating current of 1 to 2 mA delivered to the endocardium of the right ventricle, resulting in VF. Simultaneously, mechanical ventilation was discontinued.

A 13-French sheath introducer (Impella 2.5 introducer kit 13 F, 13 cm; Abiomed Europe GmbH, Aachen, Germany) was placed in the right femoral artery. A modified Impella 2.5 left ventricular assist device (Abiomed) equipped with a shortened angled cannula to meet the anatomical constraints of the animal was introduced using the vascular access into the left ventricle with the help of fluoroscopy guidance, pigtail catheter (Cordis 6 F PIG 145° 110 cm Super Torque Plus; Cordis, Miami Lakes, FL, USA) and a guidewire (Platinum Plus 0.018 in × 260 cm; Boston Scientific, Natick, MA, USA) (see Fig. 1 for details). Impella 2.5 support was activated at the maximum achievable flow ten minutes following the onset of VF. The pig was then randomized (closed envelope method) to a FiO_2 of 1.0 without any added iNO (group 0 ppm; $n=5$) versus a FiO_2 of 1.0 blended with 20 ppm of iNO (group 20 ppm; $n=5$). Therapeutic mild hypothermia was induced using 0.5L of a 6 °C cold Ringer's solution and topical application of ice bags to the groins in all animals. The blood temperature was maintained at 33 ± 1 °C. A continuous infusion of Ringer's solution was administered at 4 ml/kg/h to ensure adequate hydration.

Post cardiac arrest care

As previously described by our group [1, 2], after ROSC and weaning from the respirator, animals were brought to their cages and monitored permanently by research staff. Within 48 hr. after weaning from respirator, animals were euthanized by intravenous injection of a lethal dose of pentobarbital.

Transesophageal Echocardiography

All TEE studies were performed by the same board-certified physician at baseline (after all catheters were placed),

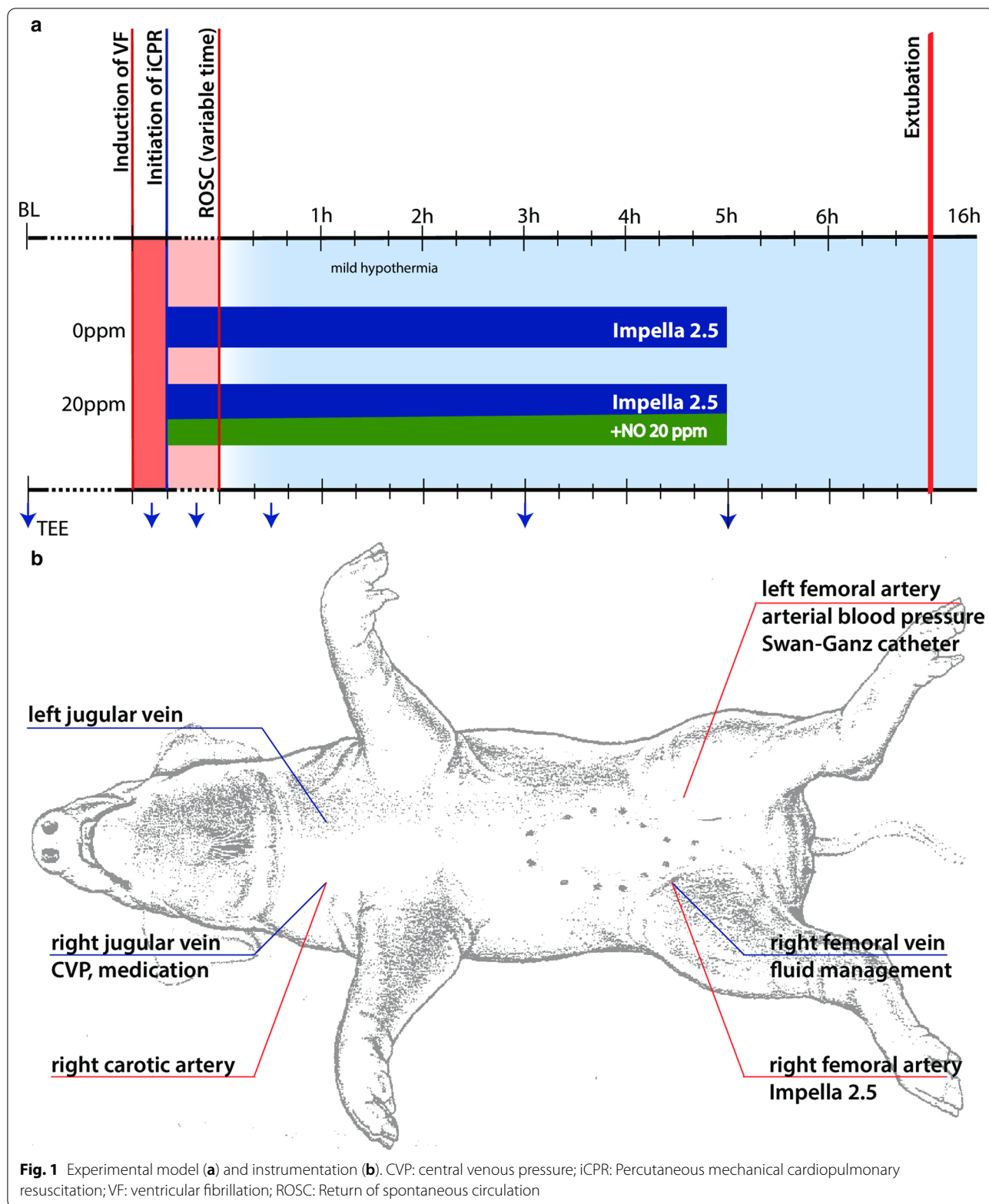
during VF and iCPR, and at 30mins, 3 h, 5 h post-ROSC. We used a commercially available ultrasound machine (Vivid E9, GE Vingmed Ultrasound AS, Horten, Norway) equipped with a 6VT-D [3.0–8.0 MHz] TEE probe. Our detailed TEE protocol in swine has been described previously [7]. In brief, at least three consecutive cardiac cycles were stored and averaged for all measurements. The analysis was carried out offline using the device's software package (EchoPAC Version 202; GE Vingmed Ultrasound AS, Horten, Norway) according to the recommendation of the European Association of Cardiovascular imaging [8]. Images were acquired from mid-esophageal, transgastric, and upper esophageal views. Valvular pathologies were excluded by color-Doppler. LV end-diastolic (LVEDV) and end-systolic (LVESV) volumes were measured in the mid-esophageal four-chamber (4-CH) views and deep esophageal two-chamber (2-CH) views. The modified biplane Simpson's method was used for Ejection fraction (EF) measurements [9]. RV fractional area change (RV-FAC) was determined according to the following formula:

$$\text{RV-FAC} = \frac{\text{End-diastolic area} - \text{end-systolic area}}{\text{End-diastolic area}} \times 100\%$$

TDI was used to measure RV peak systolic tricuspid annulus velocity (TASV) from a 4-CH view as an indicator of RV longitudinal function [10]. The PWD sample was placed in RV- (RVOT) and LV-outflow tracts (LVOT) to obtain velocity time integrals (VTI). RV Cardiac output (CO) was calculated using the formula: $\text{CO} = \text{VTI}_{\text{RVOT}} \times \text{RVOT cross-sectional area} \times \text{heart rate}$ and for the LV $\text{CO} = \text{VTI}_{\text{LVOT}} \times \text{LVOT cross-sectional area} \times \text{heart rate}$.

Speckle tracking and non-invasive myocardial work measurements:

2-D speckle-tracking (STE) was used to define LV global longitudinal strain (LV-GLS) and RV-GLS. LV GLS was measured using the three apical chamber views (4-CH, 2-CH and apical long axis (LAX)). For STE analysis of the RV the 4CH view for the RV anterior wall was used. The RV free wall was captured from a modified upper long axis view (LAX) of the RV in- and outflow tract and part of the posterior RVOT was obtained from a mid-esophageal LAX RV view (Please refer to supplementary Fig. 1 for a representative view). Aortic and mitral valve opening and closure times were determined by PWD. The systolic arterial and pulmonary blood pressures were entered into the EchoPAC software (GE Vingmed Ultrasound AS, Horten, Norway). After completing the STE analysis of LV and RV, EchoPAC calculated pressure-strain loops (PSL). Adjusted LV pressure curves corresponding



to the length of isovolumic and ejection phases were generated by EchoPAC software, as described by Russel et al. [11, 12]. The global myocardial work index (GWI) was calculated from the area within the PSL and the following parameters were then calculated from the PSL: 1) GWI: The total myocardial work from mitral valve closure to mitral valve opening is represented by the total area of PSL; 2) global constructive myocardial work (GCW): the ventricular work which contributes to the ejection during systole: $GCW = \text{positive work during systole} + \text{negative work during isovolumic relaxation}$; 3) global wasted myocardial work (GWW): the ventricular work that does not contribute to the ejection of blood. $GWW = \text{negative work during systole} + \text{positive work during isovolumic relaxation}$; 4) global myocardial work efficiency (GWE): the fraction of constructive myocardial work to total work [11–13]. LV pressure was estimated by adjusting a reference pressure curve with measured blood pressure and with echocardiography derived valvular event timing [11–13]. We used the blood pressure taken from the femoral artery for that purpose. RV's pressure was measured using the Swan-Ganz catheter. The myocardial work was expressed in mmHg%. EchoPAC provided a validated assessment of LV myocardial work indices. To our knowledge, measurements for RV myocardial work indices with EchoPAC were not validated by GE healthcare or by any other research group yet.

Statistical analysis

Statistical analysis was performed with STATA IC16 (StataCorp., TX, USA) and Jamovi project (Version 1.6.1, <https://www.jamovi.org>). Figures were created using Graph Pad Prism version 7.0a for MAC OS X (Graph Pad Software, La Jolla, California USA) and prepared for submission using Adobe® Illustrator® CS6 (Adobe Inc., San Jose, California, USA). The normal distribution of continuous variables was assessed using the Shapiro–Wilk-Test, and was expressed as mean \pm standard deviation. A mixed-effects model was used for between-group comparisons at different time-points and Sidak's test was used to account for multiple comparisons. The non-parametric Friedman-test and Dunn's correction for multiple comparisons was used for intergroup comparisons at different time points. Pearson's correlation test was performed to assess the correlation between the invasive thermodilution measured CO (CO_{TD}) and the PWD derived CO (CO_{PWD}). Adjusted p-values for multiple comparisons are presented and $p < 0.05$ was considered statistically significant.

Results

Impella controller derived flow correlates well with pulsed-wave Doppler derived flow

All 10 pigs survived 15 h post-ROSC and were successfully extubated. No complications due to TEE probe insertion or during TEE image acquisition were observed. Body surface area was similar between groups (0 ppm : 1.2 ± 0.1 vs. 20 ppm : $1.3 \pm 0.1 \text{ m}^2$, $p = 0.278$). At least two different clear views of 4-CH, 2-CH, and LAX at all given time points were obtained in all animals.

The mean heart rate at baseline was $92 \pm 14 \text{ min}^{-1}$. The systemic and pulmonary artery pressure at baseline did not differ between groups and are presented in Table 1. CO_{PWD} correlated well with the invasively measured CO_{TD} at baseline, 30 min, 3 h and 5 h ($r = 0.71$, $p = 0.021$; $r = 0.91$, $p < 0.001$; $r = 0.93$, $p < 0.001$; $r = 0.84$, $p < 0.01$, respectively) (Fig. 2). The calculated pump flow displayed by the automated Impella controller correlated well with the PWD derived pulmonary flow following iCPR initiation (1.8 ± 0.2 vs. $1.9 \pm 0.2 \text{ L/min}$, $r = 0.85$, $p = 0.012$).

Arterial blood gas analysis

An overview of arterial blood gas analysis (BGA) throughout the experiment is provided in Fig. 3 and Table 2. At baseline, all BGA parameters did not differ between the two groups. Lactate increased significantly in both groups during iCPR and 30 min following ROSC (20 ppm : baseline vs. iCPR: 1.4 ± 0.5 vs. $7.0 \pm 0.6 \text{ mmol/L}$, $p = 0.005$; 0 ppm : Baseline vs. iCPR: 1.3 ± 0.4 vs. $7.2 \pm 0.6 \text{ mmol/L}$, $p < 0.001$) and returned to baseline value 3 h post-ROSC. During and after iCPR, all BGA parameters, with exception of pO_2 and pCO_2 , did not differ between the two groups at all measured time-points. At 5 h post-ROSC, the pO_2 was significantly higher in the 20 ppm group than in the 0 ppm group (141.4 ± 9.4 vs. $102.4 \pm 15.4 \text{ mmHg}$, $p = 0.011$), and the pCO_2 was significantly lower in the 20 ppm compared to the 0 ppm group (46.1 ± 1.9 vs. $38.7 \pm 2.7 \text{ mmHg}$, $p = 0.007$).

Application of iNO significantly increases cardiac output and improves left ventricular systolic function recovery

At baseline, LVEDV, LV-EF and LV-GLS did not differ between groups. After induction of VF, LVEDV increased significantly in both groups compared to baseline (Fig. 4a). Over the course of iCPR for 5 h, LVEDV decreased and returned closer to baseline values in both groups (Fig. 4a and Table 3). However, LVEDV in the 20 ppm group was higher at all time points and was statistically significant at 3 h post-ROSC (0 ppm : 78.2 ± 1.1 vs. 20 ppm : $70.8 \pm 1.3 \text{ mL}$, $p < 0.001$). LV-EF did not differ significantly between groups at all time points or within each group compared to baseline (Fig. 4b). The

Table 1 Hemodynamic parameters before, during and after the resuscitation using a percutaneous mechanical circulatory support device

	0 ppm	20 ppm	Total	p
BSA m ²	1.2±0.1	1.3±0.1	1.3±0.1	0.271
Baseline				
HR min ⁻¹	85.6±13.9	98.4±11.6	92.0±13.8	0.152
SBP mmHg	129.2±16.5	126.4±20.3	127.8±17.5	0.817
DBP mmHg	68.6±8.6	67.4±5.9	68.0±7.0	0.805
SPAP mmHg	26.6±2.8	24.8±3.6	25.7±3.2	0.400
DPAP mmHg	14.2±2.7	12.4±2.9	13.3±2.8	0.337
CO _{PWD} L/min	6.9±1.7	7.0±0.8	7.0±1.3	0.878
CO _{TD} L/min	6.7±1.5	7.3±0.7	7.0±1.2	0.459
Cardiac arrest				
CO _{PWD} L/min	1.7±0.2	1.8±0.2	1.8±0.2	0.341
Impella flow L/min	1.9±0.3	1.9±0.2	1.9±0.2	0.892
HR _{pp-VF} min ⁻¹	20.8±1.1	21.4±0.8	21.1±0.9	0.491
30 min post-ROSC				
HR min ⁻¹	115±24.3	130±30	128±36	0.055
SBP mmHg	95.2±12.9	95.6±25.1	95.4±18.8	0.976
DBP mmHg	64.8±10.6	64.4±10.9	64.6±10.1	0.955
SPAP mmHg	26.2±3.8	25.2±6.2	25.7±4.9	0.766
DPAP mmHg	14.4±3.5	11.8±5.3	13.1±4.5	0.388
CO _{TD} L/min	5.5±1.7	5.6±1.2	5.6±1.4	0.900
CO _{PWD} L/min	5.1±1.1	5.7±1.2	5.4±1.1	0.433
3 h post-ROSC				
HR min ⁻¹	102.8±13.9	111.6±21.6	107.2±17.7	0.466
SBP mmHg	99.6±8.6	114.2±28.0	106.9±21.0	0.298
DBP mmHg	68.0±7.3	65.0±11.7	66.5±9.3	0.639
SPAP mmHg	28.0±5.5	28.4±4.6	28.2±4.8	0.903
DPAP mmHg	15.0±3.2	14.4±3.6	14.7±3.3	0.790
CO _{PWD} L/min	4.6±1.0	6.6±1.1	5.7±1.5	0.016
CO _{TD} L/min	5.1±0.8	6.8±2.3	5.9±1.8	0.172
5 h post-ROSC				
HR min ⁻¹	75.0±11.0	104.8±19.6	89.9±21.7	0.018
SBP mmHg	110.2±13.8	113.0±18.0	111.6±15.2	0.790
DBP mmHg	68.0±9.8	66.2±9.0	67.1±8.9	0.771
SPAP mmHg	32.0±4.4	23.0±1.0	27.5±5.6	0.008
DPAP mmHg	16.2±3.7	11.8±1.3	14.0±3.5	0.037
CO _{PWD} L/min	4.0±0.6	5.8±1.0	4.9±1.2	0.036
CO _{TD} L/min	3.5±0.6	5.6±1.5	4.5±1.6	0.021

CO_{PWD}: Pulsed-wave Doppler derived cardiac output; CO_{TD}: Cardiac output measured with thermodilution method using wan-Ganz catheter; DBP: Diastolic blood pressure; DPAP: Diastolic pulmonary artery pressure; HR: Heart rate; HR_{pp-VF}: Peak to peak ventilation frequency as the Heart rate during cardiac arrest; SBP: Systolic blood pressure; SPAP: Systolic pulmonary artery pressure

LV-GLS improved throughout the duration of iCPR in both groups from baseline (Fig. 4c). The LV-GLS values were significantly lower at 3 h and 5 h post-ROSC in the 20 ppm group compared to the 0 ppm group (5 h: 0 ppm: -13.1±2.4 vs. 20 ppm: -18.2±3.4, p=0.025)

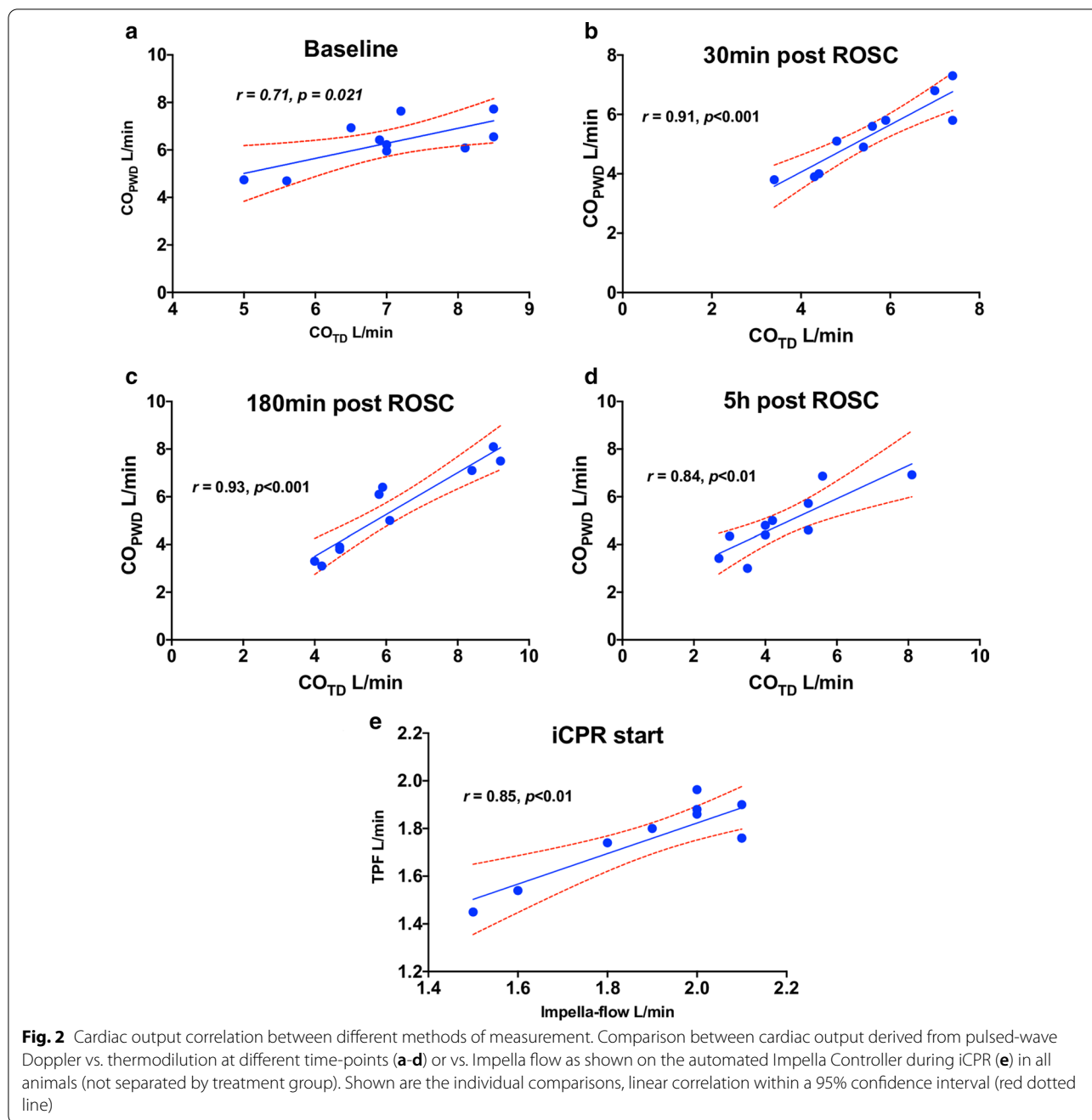
(Fig. 4c). The CO decreased in both groups at iCPR initiation and improved over the course of iCPR. The CO_{PWD} increased significantly in the 20 ppm group at 3 h and 5 h post-ROSC compared to the 0 ppm group (3 h: 0 ppm: 4.6±0.9 L/min vs. 20 ppm: 6.6±1.1, p=0.016; 5 h: 0 ppm: 4.0±0.6 L/min vs. 20 ppm: 5.8±1.0, p=0.036) (Fig. 4d).

Application of iNO enhances right ventricular systolic function recovery

RV echocardiographic measurements, RV basal diameters at end-diastole (RVEDD), RV-FAC, TASV and RV-GLS, did not differ between the two groups at baseline (Fig. 5a–d and Table 3). However, RV-FAC decreased significantly during CA and 30 min post-ROSC. In the 0 ppm group, RV-FAC was lower at all time-points compared to baseline (0 ppm baseline vs. 30 min, vs. 3 h vs. 5 h post-ROSC: 44.1±6.1% vs. 27.4±2.8%, p=0.004; vs. 32±5%, p=0.009; vs. 33.2±4.3%, p=0.001; see also Table 3). In the 20 ppm group, RV-FAC improved at 3 h and recovered to baseline values at 5 h post-ROSC (baseline: 42.9±6.6% vs. 5 h: 41.1±6.4; p=0.442) (Fig. 5a). RVEDD increased significantly in both groups at iCPR initiation, and slowly recovered over time but did not differ between groups (Fig. 5b and Table 3). Within the 0 ppm group, TASV decreased significantly after CA and remained lower during the course of iCPR (baseline vs. 3 h: 13.6±1.1 vs. 7.8±1.6 cm/s, p=0.024; baseline vs. 5 h: 13.6±1.1 vs. 9.4±1.3 cm/s, p=0.009, respectively) (Fig. 5a and Table 3). The TASV values in the 20 ppm group were higher at 3 h and 5 h post-ROSC compared to the 0 ppm group (20 ppm vs. 0 ppm at 3 h: 11.4±1.1 vs. 7.8±1.6 cm/s, p=0.024; at 5 h: 12.8±1.1 vs. 9.4±1.3 cm/s, p=0.012). The RV-GLS values were similar between the two groups at baseline and post-ROSC. However, RV-GLS at 5 h post-ROSC was significantly lower in the 20 ppm group than 0 ppm (0 ppm vs. 20 ppm at 5 h: -9±1.4% vs. -13±2.2%; p=0.007; Fig. 5d).

LV myocardial work indices indicate recovery during and after ventricular unloading

At baseline, myocardial work indices (GWI, GWE, GCW, GWW) did not differ between the two groups (Fig. 6a–d and Table 3). The LV-GWI did not differ between the two groups at any time. However, LV-GWI in the 20 ppm group recovered after an initial decrease and began to recover at 30 min post-ROSC to reach almost baseline values at 5 h post-ROSC (baseline: 1,751±270 mmHg% vs. 5 h: 1,529±274 mmHg%, p=0.401) (Fig. 6a and Table 3), while in the 0 ppm group, LV-GWI was significantly lower compared to baseline at all time-points (baseline:



1,835 ± 305 mmHg%; 30 min: 891.2 ± 412 mmHg% ($p = 0.032$), 3 h: 896 ± 129 mmHg% ($p = 0.011$), and 5 h: 1,125 ± 214 mmHg% ($p = 0.011$); Fig. 6a). LV-GWE and LV-GCW had a similar time-course to LV-GWI and did not recover in the 0 ppm group (Fig. 6b). The LV-GWW did not differ between groups and did not increase significantly in both groups at all time-points compared to baseline (Fig. 6c).

RV myocardial indices indicate a more complex pattern and slower recovery

At baseline, the RV myocardial work indices did not differ between groups (0 ppm vs. 20 ppm, Fig. 7a-c and Table 3). At 3 h and 5 h post-ROSC, RV-GWI was significantly lower in the 0 ppm group compared to the 20 ppm group (0 ppm: 108.4 ± 22.6 vs. 20 ppm: 189.6 ± 43.6 mmHg%, $p = 0.049$ and 0 ppm: 152.6 ± 42.4

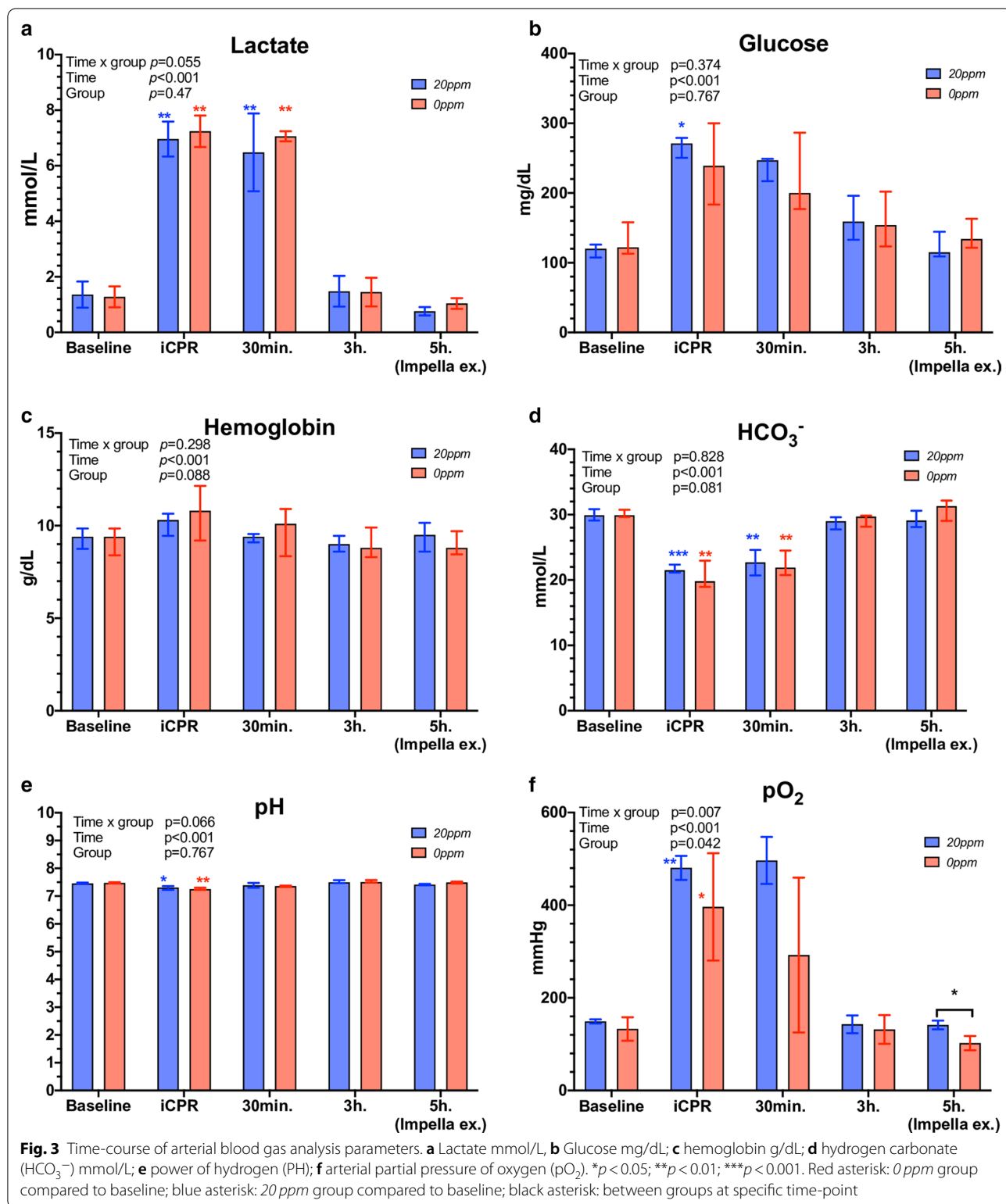


Table 2 Arterial blood gas analysis before, during and after resuscitation

	0 ppm	20 ppm	total	p
Baseline				
Lactate mmol/L	1.3 ± 0.4	1.4 ± 0.5	1.3 ± 0.4	1.000
Hemoglobin g/dL	9.2 ± 0.8	9.3 ± 0.6	9.2 ± 0.7	0.834
Glucose mg/dL	132.8 ± 24.6	117.4 ± 9.7	125.1 ± 19.4	0.465
pH	7.48 ± 0.02	7.46 ± 0.01	7.47 ± 0.02	0.251
HCO ₃ mmol/L	30.1 ± 0.6	30.0 ± 1.1	30.1 ± 0.8	0.751
BE mmol/L	6.1 ± 0.8	6.1 ± 1.1	6.1 ± 0.9	0.600
pO ₂ mmHg	132.8 ± 25.4	149.2 ± 4.4	141.0 ± 19.2	0.251
pCO ₂ mmHg	43.3 ± 2.4	39.8 ± 2.4	41.5 ± 2.9	0.057
iCPR				
Lactate mmol/L	7.2 ± 0.6	7.0 ± 0.6	7.1 ± 0.6	0.402
Hemoglobin g/dL	10.7 ± 1.5	10.1 ± 0.7	10.4 ± 1.1	0.465
Glucose mg/dL	241.2 ± 63.2	266.0 ± 17.6	253.6 ± 45.6	0.754
pH	7.26 ± 0.03	7.29 ± 0.07	7.27 ± 0.05	0.347
HCO ₃ mmol/L	20.7 ± 2.1	21.7 ± 0.6	21.2 ± 1.5	0.602
BE mmol/L	-4.1 ± 2.4	-3.6 ± 1.6	-3.8 ± 1.9	0.917
pO ₂ mmHg	396.4 ± 115.7	480.6 ± 25.9	438.5 ± 90.7	0.117
pCO ₂ mmHg	47.3 ± 8.3	50.4 ± 4.0	48.8 ± 6.3	0.465
30 min post ROSC				
Lactate mmol/L	7.1 ± 0.2	6.5 ± 1.4	6.8 ± 1.0	0.116
Hemoglobin g/dL	9.7 ± 1.3	9.3 ± 0.3	9.5 ± 0.9	0.600
Glucose mg/dL	225.4 ± 57.3	235.8 ± 20.2	230.6 ± 40.9	0.602
pH	7.39 ± 0.07	7.35 ± 0.1	7.37 ± 0.07	0.142
HCO ₃ mmol/L	22.5 ± 1.9	22.7 ± 2.3	22.6 ± 2.0	0.754
BE mmol/L	-2.5 ± 1.7	-1.6 ± 2.7	-2.1 ± 2.2	0.463
pO ₂ mmHg	292.4 ± 167.1	496.6 ± 50.7	394.5 ± 158.5	0.028
pCO ₂ mmHg	39.4 ± 9.3	41.8 ± 2.5	40.6 ± 6.5	0.602
3 h post ROSC				
Lactate mmol/L	1.4 ± 0.5	1.5 ± 0.6	1.5 ± 0.5	0.530
Hemoglobin g/dL	9.0 ± 0.8	9.0 ± 0.4	9.0 ± 0.6	0.917
Glucose mg/dL	161.0 ± 51.1	163.4 ± 37.4	162.2 ± 42.3	0.602
pH	7.53 ± 0.05	7.51 ± 0.05	7.52 ± 0.05	0.465
HCO ₃ mmol/L	29.1 ± 1.0	28.7 ± 1.2	28.9 ± 1.1	0.402
BE mmol/L	4.9 ± 1.2	4.8 ± 1.4	4.8 ± 1.2	1.000
pO ₂ mmHg	131.7 ± 31.1	143.0 ± 19.2	137.4 ± 25.1	0.402
pCO ₂ mmHg	34.4 ± 5.6	33.3 ± 5.6	33.9 ± 5.3	0.917
5 h post ROSC				
Lactate mmol/L	1.0 ± 0.2	0.8 ± 0.2	0.9 ± 0.2	0.139
Hemoglobin g/dL	9.0 ± 0.8	9.4 ± 0.9	9.2 ± 0.8	0.401
Glucose mg/dL	140.6 ± 22.1	124.4 ± 24.4	132.5 ± 23.6	0.249
pH	7.49 ± 0.02	7.42 ± 0.03	7.45 ± 0.04	0.050
HCO ₃ mmol/L	30.7 ± 1.7	29.3 ± 1.3	30.0 ± 1.6	0.175
BE mmol/L	7.2 ± 1.7	6.0 ± 1.6	6.6 ± 1.7	0.251
pO ₂ mmHg	102.4 ± 15.4	141.4 ± 9.4	121.9 ± 23.9	0.010
pCO ₂ mmHg	46.1 ± 1.9	38.7 ± 2.7	42.4 ± 4.4	0.007

BE: Base excess mmol/L; HCO₃⁻: Hydrogen carbonate mmol/L; pH: Power of Hydrogen; pO₂: arterial partial pressure of oxygen mmHg; pCO₂: arterial partial pressure of carbon dioxide mmHg

vs. 261.6 ± 54.2 mmHg%, $p=0.041$, respectively). Within the 0 ppm group, the RV-GWI did not recover and remained significantly decreased at 30 min, 3 h and 5 h post-ROSC compared to baseline (baseline: 338.2 ± 45.3 mmHg% vs. 30 min: 101.6 ± 34.5 mmHg%, $p<0.001$; vs. 3 h: 108.4 ± 22.6 mmHg%, $p<0.001$; vs. 5 h: 152.6 ± 42.4 mmHg%, $p=0.012$, respectively; Fig. 7b). In both groups, the RV-GCW decreased significantly after CA, but a slow recovery over time was noted in both groups with no difference between groups (Fig. 7b and Table 3). The RV-GWW increased significantly in the 0 ppm group compared to the 20 ppm group at 3 h and 5 h post-ROSC: 69.6 ± 11.9 vs. 47.4 ± 6.7, $p=0.049$ and 77.8 ± 14.8 vs. 50.2 ± 8.2, $p=0.046$, respectively (Fig. 7c). The RV-GWE increased significantly in the 20 ppm group at 5 h post-ROSC compared to the 0 ppm group (80 ± 5.2 vs. 73 ± 5.7, $p=0.042$, respectively).

Diagnostic utilization of pressure-strain loops

Figure 8a is a representative overlay of the PS-loops of the LV. An acute injury following iCPR initiation is demonstrated by narrowing of the PS-loop (a sign of loss in maximally generated strain), thus explaining the ventricle's inability to generate sufficient pressure [14–18].

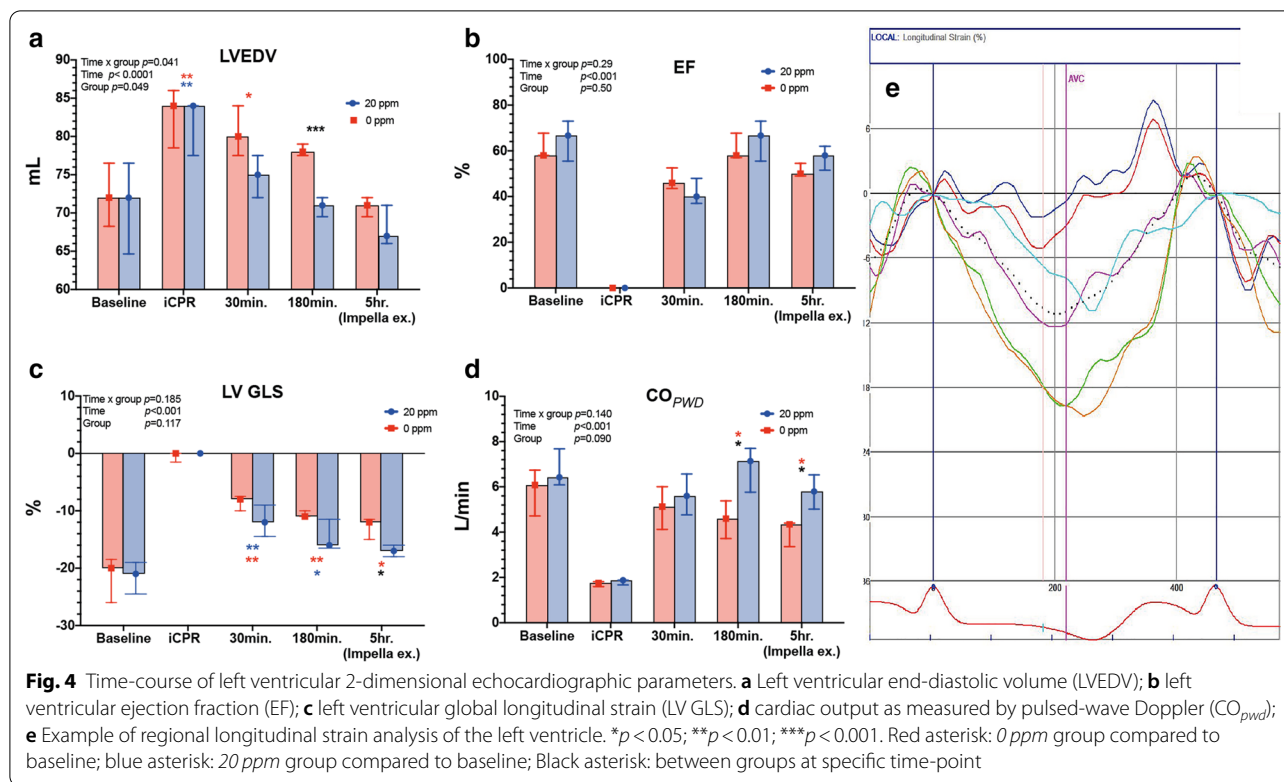
The partially positive strain indicates a passive distention of the myocardium due to volume loading [16–18]. Unloading leads to slow recovery and progressive normalization of the PS-loop, which remains below (i.e., less negative) normal values but shows a curve pattern comparable to normal conditions [18, 19].

Figure 8b is a representative overlay of the PS-loops of the right ventricle. A pumping failure leads to increased RVP, and a loss in strain translates to a more complex strain-pressure relation [20, 21]. The RV strain reduction remains pronounced even after a longer duration of left ventricular support [21, 22].

Figure 8c demonstrates the spatial distribution of strain at different time-points. This allows differentiation of regional wall motion deterioration e.g., in acute myocardial infarction from global failure, thus providing a detailed perspective on myocardial recovery over time.

Discussion

Resuscitation following cardiac arrest remains associated with significant mortality and morbidity [23]. Although treatment guidelines recommend inotropes and vasopressors, many studies have demonstrated their detrimental side effects [23]. In the early phase of resuscitation, treatments aim to augment or stabilize cardiac output, allowing minimal end-organ perfusion, and reducing or preventing hypoxic/ischemic injury [12–14].



However, these treatments cause increased myocardial stress and oxygen demand when oxygen supply is low [24, 25].

Trans-valvular mechanical support devices like the Impella device family uncouple the myocardial workload from the systemic cardiac output (which is then primarily provided by the pump), leading to adequate end-organ perfusion while resting the heart [3, 26]. Previous studies [27–29] have demonstrated the efficacy of this intravascular resuscitation, and the present study in an animal model confirms the results and provides additional insights on the temporal evolution of the effect.

Global myocardial work and the principle of unloading

The pressure-strain (PS) loop generated by tracking the global myocardial strain vs. the LVEDP/RVEDP over the cardiac cycle provides a momentary impression of the myocardial work and is comparable to the pressure–volume (PV) loops derived from conductance catheters [4, 11, 12]. Russel et al. [11, 12] demonstrated a strong correlation between the non-invasive LV PS-loop area and the invasive PV-loop area. The LV PV-loop analysis considers the LV load and has been shown in experimental studies to be a reliable and robust method for quantifying LV performance. Moreover, the PV-loop area provides valuable information on the myocardial O_2 -consumption [30,

31]. Despite being a valuable and reliable method, the PV-loop method is not used in clinical practice due to its invasiveness [11, 12, 32, 33].

Evaluation of ventricular function is an essential component of all echocardiographic examinations. Despite the many LVEF measurement limitations, LVEF remains the most widely used parameter for systolic function evaluation [34]. More recently, the peak longitudinal strain from 2D-speckle tracking analysis has gained acceptance in the clinical routine. Compared to EF, GLS can detect subclinical myocardial abnormalities. However, GLS analysis suffers from load dependency and has limitations [35].

The PS-loop analysis incorporates both the deformation changes and afterload, thus overcoming the limitations of load dependency [4]. Therefore, GWI provides incremental information to EF and GLS analysis. While the PV-loop area reflects myocardial metabolic demand and oxygen consumption, the non-invasive myocardial work method provides myocardial energetics [11, 12, 33]. For several decades, stroke work evaluation played a key role in heart failure characterization and decision-making regarding optimal treatment. Traditional stroke work measurements are calculated using the LV PV-loop area derived from invasive catheterization [30, 31]. The PS-loop method has a robust correlation with invasive

Table 3 Comparison of echocardiographic parameters between the groups with and without inhaled nitric oxide

	0 ppm	20 ppm	Total	p
Baseline				
RVD1 cm	3.1 ± 0.4	3.4 ± 0.4	3.3 ± 0.4	0.332
RVD2 cm	2.6 ± 0.2	2.7 ± 0.4	2.6 ± 0.3	0.417
RVD3 cm	4.0 ± 0.2	3.8 ± 0.4	3.9 ± 0.3	0.424
RV-FAC %	44.1 ± 6.0	42.9 ± 6.6	43.5 ± 6.0	0.772
LVEDV mL	70.5 ± 3.5	70.9 ± 6.1	70.7 ± 4.7	0.911
LVESV mL	31.9 ± 4.6	33.4 ± 3.6	32.6 ± 4.0	0.583
LV-EF %	61.5 ± 5.8	64.7 ± 9.2	63.1 ± 7.5	0.525
LV-GLS %	-21.0 ± 5.1	-21.6 ± 3.4	-21.3 ± 4.1	0.833
LV-GWI mmHg%	1835.3 ± 306.2	1751 ± 270.2	3444.3 ± 5242.8	0.336
LV-GCW mmHg%	2095.8 ± 527.4	2103.2 ± 405.8	2099.5 ± 443.6	0.981
LV-GWW mmHg%	368.0 ± 208.8	352.4 ± 115.9	360.2 ± 159.4	0.887
LV-GWE %	85.2 ± 4.7	80.0 ± 1.4	82.6 ± 4.2	0.054
TASV cm/sec	13.6 ± 1.1	13.8 ± 1.5	13.7 ± 1.3	0.817
RV-GLS %	-16.4 ± 3.2	-14.4 ± 1.8	-15.4 ± 2.7	0.267
RV-GWI mmHg%	338.2 ± 45.3	286.8 ± 57.5	312.5 ± 55.8	0.155
RV-GCW mmHg%	376.4 ± 92.6	266.6 ± 41.1	321.5 ± 89.0	0.082
RV-GWW mmHg%	61.6 ± 13.8	55.4 ± 10.6	58.5 ± 12.1	0.949
RV-GWE %	79.8 ± 10.2	80.8 ± 6.1	80.3 ± 7.9	0.855
Cardiac arrest				
RVD1 cm	4.0 ± 0.3	4.2 ± 0.3	4.1 ± 0.3	0.397
RVD2 cm	3.3 ± 0.6	3.5 ± 0.4	3.4 ± 0.5	0.581
RVD3 cm	4.5 ± 0.2	4.6 ± 0.5	4.6 ± 0.4	0.749
RVEDA cm ²	13.9 ± 1.6	15.2 ± 1.1	14.6 ± 1.4	0.183
LVEDV mL	81.0 ± 4.9	76.6 ± 7.5	78.8 ± 6.4	0.306
30 min. post-ROSC				
RVD1 cm	3.7 ± 0.3	3.6 ± 0.4	3.7 ± 0.3	0.582
RVD2 cm	3.0 ± 0.4	2.9 ± 0.4	2.9 ± 0.4	0.716
RVD3 cm	4.5 ± 0.2	4.6 ± 0.1	4.5 ± 0.2	0.776
RV-FAC %	27.4 ± 2.8	32.0 ± 9.3	30.5 ± 6.5	0.494
LVEDV mL	77.0 ± 6.5	73.8 ± 9.7	75.4 ± 8.0	0.558
LVESV mL	35.8 ± 5.1	35.4 ± 3.7	35.6 ± 4.2	0.897
LVEF %	47.6 ± 5.0	42.0 ± 8.1	44.8 ± 7.0	0.225
LV-GLS %	-11.6 ± 3.3	-13.2 ± 4.7	-12.4 ± 3.9	0.548
LV-GWI mmHg%	891.2 ± 412.7	1201.8 ± 400.5	1046.5 ± 416.8	0.262
LV-GCW mmHg%	719.0 ± 497.8	919.6 ± 638.2	819.3 ± 549.8	0.595
LV-GWW mmHg%	360.4 ± 271.1	240.2 ± 148.1	300.3 ± 215.4	0.416
LV-GWE %	63.4 ± 7.7	75.0 ± 8.7	69.2 ± 9.9	0.256
TASV cm/sec	10.4 ± 4.9	9.8 ± 1.8	10.1 ± 3.5	0.803
RV-GLS %	-6.6 ± 3.3	-9.4 ± 2.9	-8.0 ± 3.3	0.193

Table 3 (continued)

	0 ppm	20 ppm	Total	p
RV-GWI mmHg%	101.6 ± 34.5	92.0 ± 33.3	96.8 ± 32.4	0.666
RV-GCW mmHg%	152.2 ± 15.5	159.6 ± 20.2	164.1 ± 40.0	0.395
RV-GWW mmHg%	59.4 ± 11.9	49.4 ± 9.1	52.3 ± 13.2	0.843
RV-GWE %	70.6 ± 12.0	74.0 ± 8.6	72.3 ± 10.0	0.621
3 h. post-ROSC				
RVD1 cm	3.3 ± 0.3	3.4 ± 0.3	3.4 ± 0.3	0.782
RVD2 cm	2.7 ± 0.3	2.8 ± 0.1	2.8 ± 0.2	0.347
RVD3 cm	4.4 ± 0.1	4.3 ± 0.3	4.3 ± 0.2	0.718
RV-FAC %	32.5 ± 5.0	43.3 ± 7.0	43.2 ± 6.8	0.945
LVEDV mL	78.2 ± 1.1	70.8 ± 1.3	74.5 ± 4.1	<0.001
LVESV mL	38.0 ± 4.9	35.2 ± 3.5	36.6 ± 4.3	0.342
LVEF %	61.5 ± 5.8	64.7 ± 9.2	63.1 ± 7.5	0.525
LV-GLS %	-12.2 ± 2.8	-16.0 ± 2.3	-14.1 ± 3.1	0.058
LV-GWI mmHg%	896.2 ± 129.3	1399.2 ± 347.3	1147.7 ± 362.4	0.116
LV-GCW mmHg%	719.0 ± 497.8	1598.8 ± 849.2	1158.9 ± 803.5	0.081
LV-GWW mmHg%	264.6 ± 78.9	293.4 ± 212.5	279.0 ± 151.9	0.784
LV-GWE %	67.2 ± 3.3	81.4 ± 5.6	74.3 ± 8.7	0.010
TASV cm/sec	7.8 ± 1.6	11.4 ± 1.1	11.0 ± 1.5	0.024
RV-GLS %	-10.0 ± 1.0	-12.0 ± 2.7	-11.0 ± 2.2	0.164
RV-GWI mmHg%	108.4 ± 22.6	189.6 ± 43.6	149.0 ± 53.9	0.049
RV-GCW mmHg%	203.4 ± 39.6	221.2 ± 85.6	212.3 ± 63.6	0.684
RV-GWW mmHg%	69.6 ± 11.9	47.4 ± 6.7	47.8 ± 13.3	0.049
RV-GWE %	72.2 ± 14.0	75.0 ± 11.1	73.6 ± 12.0	0.734
5 h post-ROSC				
RVD1 cm	3.5 ± 0.5	3.9 ± 0.7	3.7 ± 0.6	0.308
RVD2 cm	2.8 ± 0.4	3.2 ± 0.7	3.0 ± 0.6	0.287
RVD3 cm	4.4 ± 0.2	4.6 ± 0.1	4.5 ± 0.2	0.024
RV-FAC %	33.2 ± 4.3	41.1 ± 6.5	37.1 ± 6.7	0.053
LVEDV mL	70.8 ± 1.3	68.2 ± 2.7	69.5 ± 2.4	0.087
LVESV mL	38.0 ± 6.9	35.6 ± 4.5	36.8 ± 5.6	0.525
LVEF %	51.4 ± 3.0	57.0 ± 6.2	54.2 ± 5.5	0.108
LV-GLS %	-13.0 ± 2.4	-18.2 ± 3.4	-15.6 ± 3.9	0.036
LV-GWI mmHg%	1125 ± 214	1529.2 ± 274.5	1251.3 ± 348.4	0.052
LV-GCW mmHg%	1203.8 ± 253.0	1728.4 ± 466.7	1466.1 ± 449.1	0.058
LV-GWW mmHg%	395.4 ± 159.4	367.0 ± 87.2	381.2 ± 122.1	0.736
LV-GWE %	75.8 ± 2.3	82.6 ± 4.0	79.2 ± 4.7	0.071
TASV cm/s	9.4 ± 1.3	12.8 ± 1.1	9.9 ± 2.2	0.012
RV-GLS %	-9.0 ± 1.4	-13.2 ± 2.2	-11.1 ± 2.8	0.040
RV-GWI mmHg%	152.6 ± 42.4	261.6 ± 54.2	207.1 ± 73.5	0.041

Table 3 (continued)

	0 ppm	20 ppm	Total	p
RV-GCW mmHg%	224.4 ± 158.7	212.6 ± 53.8	218.5 ± 111.9	0.879
RV-GWW mmHg%	77.8 ± 14.8	50.2 ± 8.2	61.4 ± 22.4	0.046
RV-GWE %	68 ± 5.7	80 ± 5.2	76 ± 5.4	0.042

GCW: Global constructed myocardial work; GLS: Global longitudinal strain; GWE: Global myocardial work efficiency; GWI: Global myocardial work index; GWW: Global wasted work; LV: Left ventricle; LVEDV: Left ventricle end-diastolic volume; LVEF: Left ventricular ejection fraction; LVESV: Left ventricular end-systolic volume; RVEDA: right ventricle end-diastolic area; RVD1: right ventricle basal diameter from apical 4 chamber view; RVD2: right ventricular mid diameter at midlevel from apical 4 chamber view; RVD3: right ventricle longitudinal diameter; RV-FAC: right ventricular fractional area change; TASV: Tricuspid annular systolic velocity

PV-loops and enables evaluating myocardial wasted work and work efficiency [12].

The value and clinical implications of non-invasively estimated myocardial work indices have been tested in several clinical entities. Recently, Galli et al. [36] demonstrated the value of GWW and GWI in providing details on dyssynchronous contraction and segmental work. The authors [36] identified, that responders to cardiac resynchronization therapy have a higher GCW than non-responders. Using GWI and GWW enabled the early identification of patients with acute coronary occlusion with non-ST-elevation [4]. Ischemia induces changes in myocardial contraction, and it has been shown that patients with subclinical ischemia have a dyssynchronous contraction and increased GWW [15].

Secondary right ventricular failure can aggravate cardiogenic shock [37, 38]. Thus, prevention of right ventricular distension might play a crucial role in limiting progression to right ventricular failure, even during intravascular resuscitation [38]. Notably, the right ventricular preload is increased during left ventricular mechanical

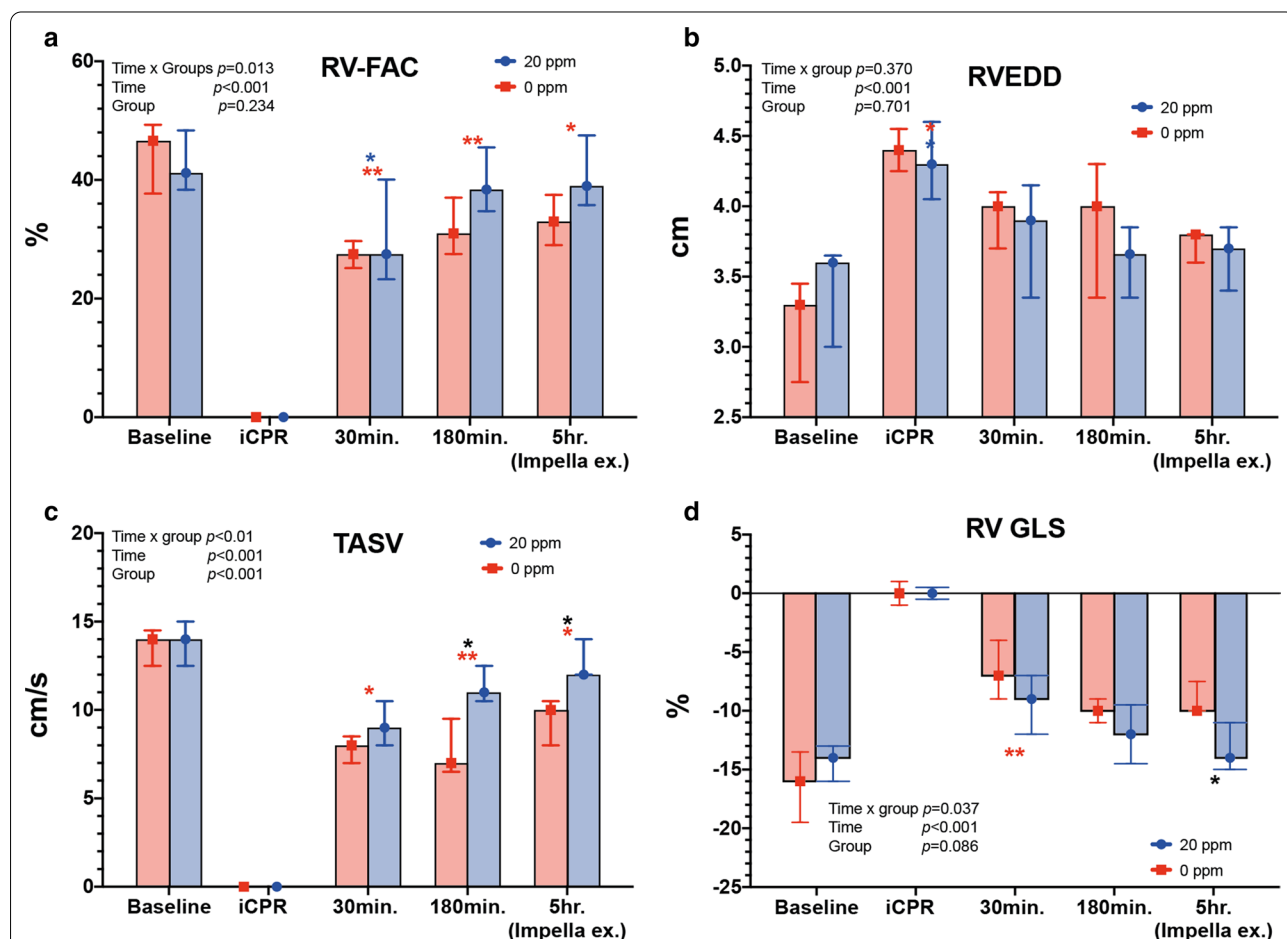
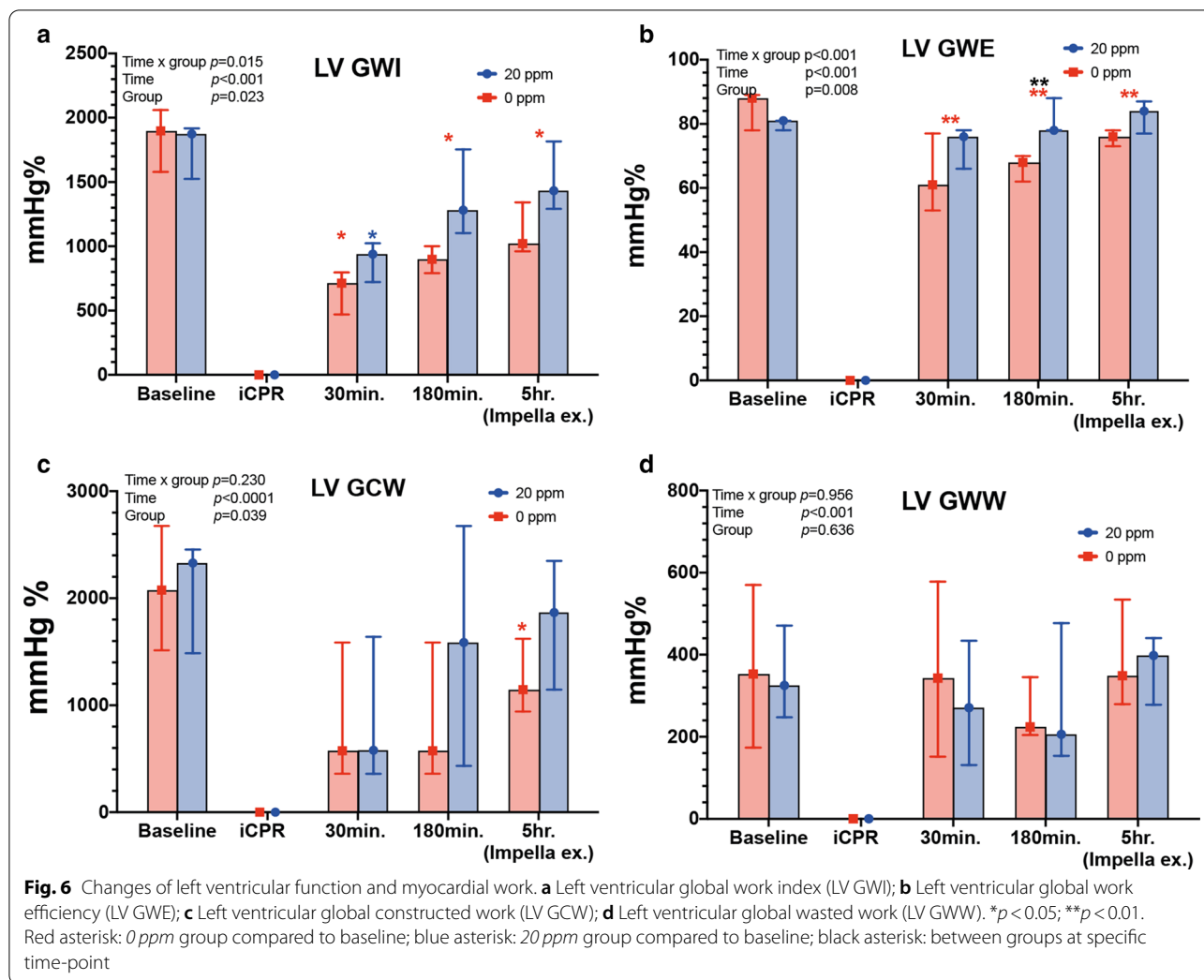


Fig. 5 Time-course of right ventricular 2-dimensional echocardiographic parameters. **a** Right ventricular fractional area change (RV-FAC); **b** Right ventricular end-diastolic diameter (RVEDD); **c** Tricuspid annular systolic velocity (TASV); **d** right ventricular global longitudinal strain (RV GLS). * $p < 0.05$; ** $p < 0.01$. Red asterisk: 0 ppm group compared to baseline; blue asterisk: 20 ppm group compared to baseline; black asterisk: between groups at specific time-point



support [39]. Transvalvular LV pumps depend on left ventricular preload to prevent suction and allow for optimal flows [39, 40]. Reduction in right ventricular afterload by pulmonary vasodilatation, leading to a decrease in pulmonary vascular resistance, should facilitate the reduction of left ventricular filling and right ventricular myocardial workload [41, 42]. The results of this study confirmed that iNO successfully decreases right ventricular afterload, normalizes RV filling pressure over time, and shifts the RV strain towards a normal (i.e., baseline) configuration.

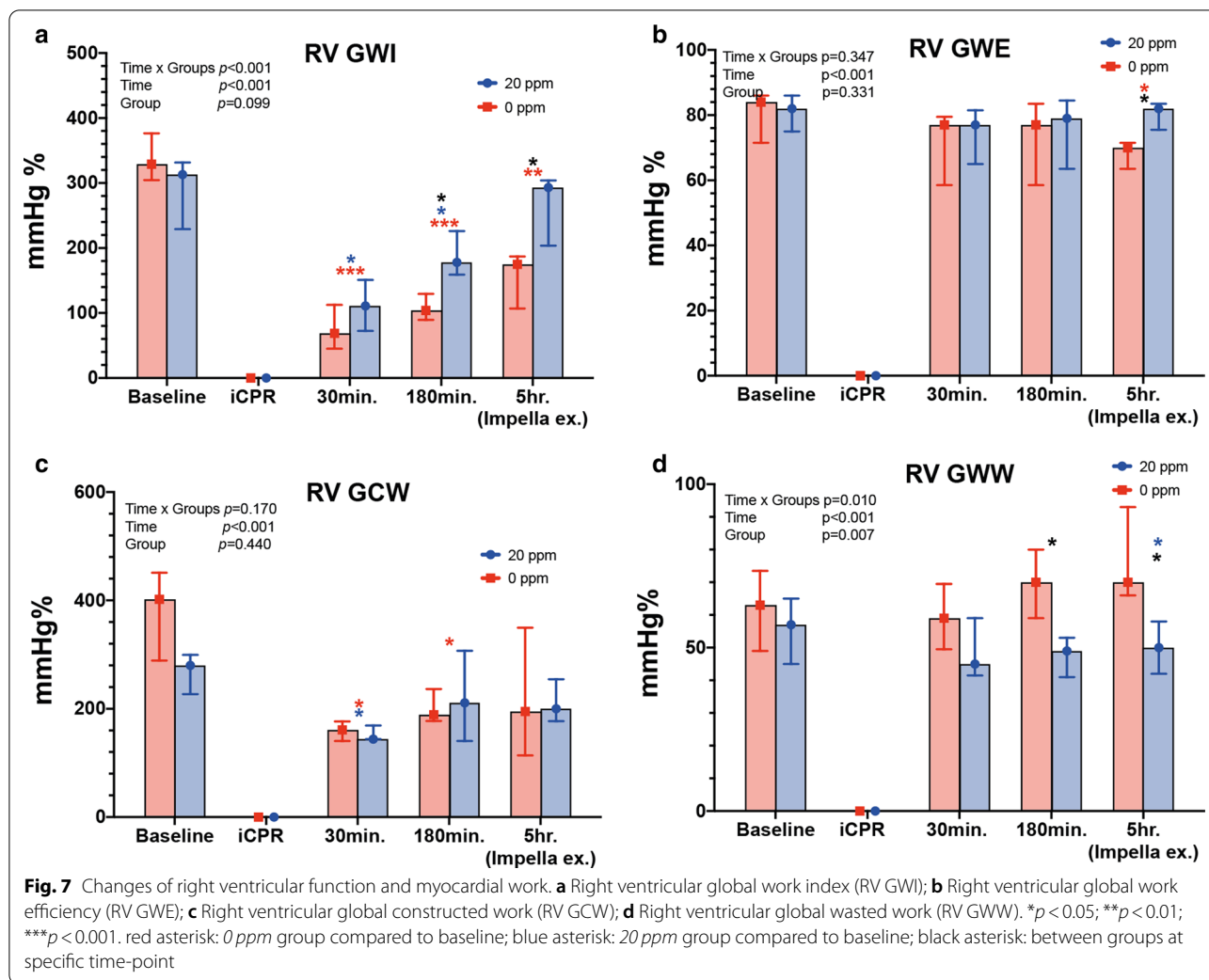
Further application perspectives of the GWI

The PS-loop method may enable an accurate ventricular-arterial coupling (VAC) analysis as it overcomes some of the limitations of traditional non-invasive methods’ used to calculate the ratio of arterial to ventricular end-systolic

elastance (Ea/Ees) [43]. The VAC impersonates an essential task in cardiac and aortic mechanics [43, 44]. The VAC evaluation has an independent diagnostic and prognostic value and can be used to refine risk stratification and monitor therapeutic interventions [43]. Cardiac arrest via myocardial hypoxia induces myocardial edema and therefore increased myocardial stiffness, thus changing Ea/Ees ratio and VAC, respectively. Therefore, the non-invasive GWI and VAC assessment might be a valuable tool in the acute phase to guide the pharmacological management of these patients.

Limitations

The small sample size of the study limits the significance of our analysis as it was not adequately powered for multiple comparisons. However, from an ethical perspective, the downsizing of experimental groups



is part of the 3R strategy. The TEE measurements in swine are challenging due to specific anatomic features. Special attention was paid to avoid foreshortening of the left ventricle in echocardiography, and ante- and retroflexion of the tip was used to correctly identify the apex of the heart. Despite all the precautions, foreshortened ventricle views might have underestimated the left ventricular volumes including the stroke volume, RV D₃ and RV areas. 3D-TEE is believed to overcome these limitations and would have led to a more precise calculation of the derived parameters. The image quality of two-chamber-views can be limited due to swine anatomy (the bronchus partially conceals the heart from the esophagus). There are no studies comparing RV PS-loops with invasive PV-loops, to the best of our knowledge, due to lack of specific software for RV myocardial work assessment. We used the commercially available LV software provided by GE for RV myocardial work measurements.

Therefore, the results must be interpreted with caution. The peripheral arterial pressure was used for PS-loop evaluation, which might be lower than the central arterial due to a lack of pressure augmentation.

Conclusions

During resuscitation from cardiac arrest, iCPR provides sufficient unloading and preservation of end-organ perfusion by maintaining cardiac output and improving myocardial work recovery. The addition of inhaled nitric oxide enables improved preservation of RV function as determined by better recovery of RV global work indices. Myocardial work estimation by echocardiographic analysis can help understand and guide both left and right ventricular unloading to minimize myocardial stress and oxygen demand, while maintaining sufficient end-organ perfusion.

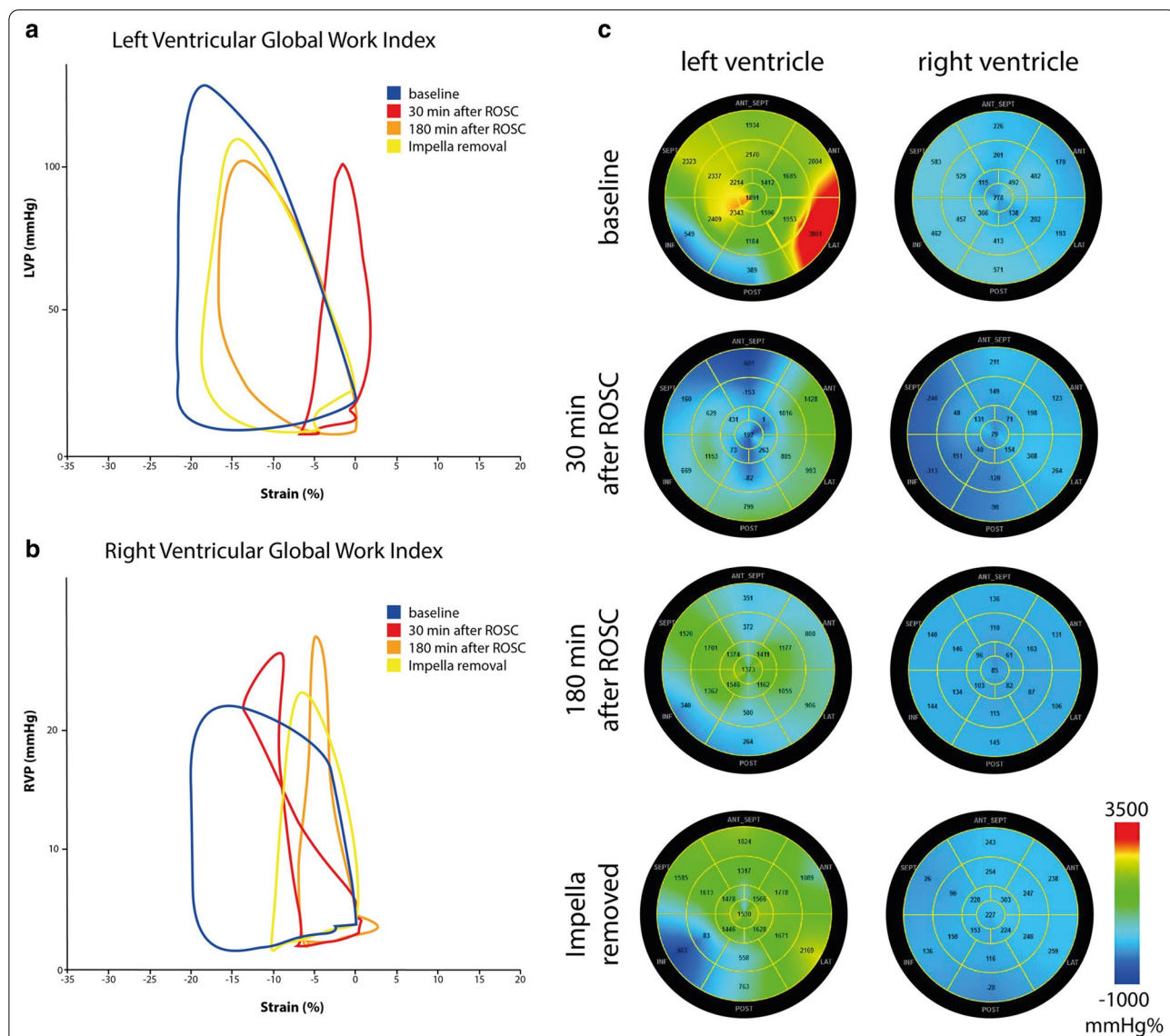


Fig. 8 Exemplary demonstration of global myocardial work index changes during the experiment. **a, b** relation of left/right ventricular pressure to global left/right ventricular strain over time. Comparable to a PV-loop, this allows to gain insights on myocardial workload and function. **c** example of spatial distribution of right and left ventricular myocardial work index. Myocardial work indices are color coded from red to blue, where red color indicate the maximum value and blue the lowest myocardial work index value

Abbreviations

CA: Cardiac arrest; CO_{PWD}: Cardiac output as measured by pulsed-wave Doppler; CO_{TD}: Cardiac output measured with thermodilution method using Swan-Ganz catheter; DBP: Diastolic blood pressure; DPAP: Diastolic pulmonary artery pressure; GCW: Global constructed myocardial work; GLS: Global longitudinal strain; GWE: Global myocardial work efficiency; GWI: Global myocardial work index; GWW: Global wasted work; HR: Heart rate; HR_{pp-vf} min⁻¹: Peak to peak inspiration frequency as the heart rate during cardiac arrest; iCPR: Percutaneous mechanical cardiopulmonary resuscitation; iNO: Inhaled nitric oxide; LAX: Apical long axes view; LV: Left ventricle; LVEDV: Left ventricular end-diastolic volume; LVEF: Left ventricular ejection fraction; LVEDP: Left ventricular diastolic pressure; LVOT: Left ventricular outflow tracts; PSL: Pressure strain loop; PV-loop: Pressure–volume loop; PWD: Pulsed-wave Doppler; ROSC: Return of spontaneous circulation; RV: Right ventricle; RVEDD: Right ventricular end-diastolic diameter; RVEDP: Right ventricular diastolic pressure;

RVD1: Right ventricle basal diameter; RVD2: Mid right ventricle diameter; RV3: Longitudinal right ventricle diameter; RV-FAC: Right ventricular fractional area change; RVOT: Right ventricular outflow tracts; SBP: Systolic blood pressure; SPAP: Systolic pulmonary artery pressure; STE: 2-D speckle-tracking echocardiography; TASV: Tricuspid annular systolic velocity; TD: Tissue Doppler imaging; TEE: Transesophageal echocardiography; VAC: Ventricular-arterial coupling; VTI: Velocity time integrals.

Acknowledgements

Not applicable.

Authors' contributions

CN and RZ contributed equally in experiments implementation, data collection, data analysis and share first authorship. MD and NH contributed equally in study conception and design, supervision, assessment of the study quality,

interpretation of the analysis and share last (senior) authorship. CN wrote the first version of the paper and drafted the manuscript. MD, NH, RR conception and study design. CN, AE, AG, MD, RZ carried out the experiments, participated in the data acquisition. RZ, NH performed and analyzed the echocardiographic studies. CN, AE, NH, RZ collected and analyzed the data. AG, MD, NH, RR, UM Interpretation of the analysis. All authors critically revised the manuscript for important intellectual content. All authors have approved the submitted version.

Funding

Open Access funding enabled and organized by Projekt DEAL. This work was supported by the German Research Foundation (Deutsche Forschungsgemeinschaft, DFG) [Grant Number DE 1685/3–1]. MD received unrestricted educational research grants and travel allowances from Abiomed Europe. The sponsor was not involved in study design; in the collection, analysis and interpretation of data; in the writing of the report; and in the decision to submit the article for publication.

Availability of data and materials

The datasets used or analyzed during the current study are available from the corresponding author on reasonable request.

Declarations

Ethics approval and consent to participate

The experimental protocol was approved by the appropriate governmental institution (Landesamt für Natur, Umwelt und Verbraucherschutz NRW (LANUV), Recklinghausen, Germany) Az.: 84–02.04.2017.A300. Written informed consent was obtained from the institute for Laboratory Animal Research, University Hospital RWTH Aachen, Germany to use the animals in our study.

Consent for publication

Not applicable.

Competing interests

AG and CN are full-time employee of Abiomed Europe GmbH, Germany. UM is a full-time employee Inc., USA. All other authors declare no competing interests.

Author details

¹ Department of Anesthesiology, Medical Faculty, RWTH University Hospital Aachen, RWTH Aachen University, 52074 Aachen, Germany. ² Abiomed Europe GmbH, Aachen, Germany. ³ Department of Thoracic and Cardiovascular Surgery, Medical Faculty, RWTH University Hospital Aachen, RWTH Aachen University, 52074 Aachen, Germany. ⁴ Abiomed, Inc., Danvers, MA, USA.

Received: 2 December 2020 Accepted: 7 April 2021

Published online: 17 April 2021

References

- Derwall M, Brücken A, Bleilevens C, Ebeling A, Föhr P, Rossaint R, Kern KB, Nix C, Fries M. Doubling survival and improving clinical outcomes using a left ventricular assist device instead of chest compressions for resuscitation after prolonged cardiac arrest: a large animal study. *Crit Care*. 2015;19(1):123.
- Derwall M, Ebeling A, Nolte KW, Weis J, Rossaint R, Ichinose F, Nix C, Fries M, Brücken A. Inhaled nitric oxide improves transpulmonary blood flow and clinical outcomes after prolonged cardiac arrest: a large animal study. *Crit Care*. 2015;19(1):328.
- Curran J, Burkhoff D, Klöner RA. Beyond reperfusion: acute ventricular unloading and cardioprotection during myocardial infarction. *J Cardiovasc Transl Res*. 2019;12(2):95–106.
- Boe E, Russell K, Eek C, Eriksen M, Remme EW, Smiseth OA, Skulstad H. Non-invasive myocardial work index identifies acute coronary occlusion in patients with non-ST-segment elevation-acute coronary syndrome. *Eur Heart J Cardiovasc Imaging*. 2015;16(11):1247–55.
- Percie du Sert N, Hurst V, Ahluwalia A, Alam S, Avey MT, Baker M, Browne WJ, Clark A, Cuthill IC, Dirnagl U, et al. The ARRIVE guidelines 2.0: Updated guidelines for reporting animal research. *PLoS Biol*. 2020;18(7):e3000410.
- Al-Rashid F, Nix C, Erbel R, Kahler P. Tools & techniques - clinical: percutaneous catheter-based left ventricular support using the Impella CP. *EuroIntervention*. 2015;10(10):1247–9.
- Billig S, Zayat R, Ebeling A, Steffen H, Nix C, Hatam N, Schnöring H, Derwall M: Transesophageal echocardiography in swine: evaluation of left and right ventricular structure, function and myocardial work. *Int J Cardiovasc Imaging* 2020.
- Flachskampf FA, Wouters PF, Edvardsen T, Evangelista A, Habib G, Hoffman P, Hoffmann R, Lancellotti P, Pepi M. Recommendations for transoesophageal echocardiography: EACVI update 2014. *Eur Heart J Cardiovasc Imaging*. 2014;15(4):353–65.
- Lang RM, Badano LP, Mor-Avi V, Afilalo J, Armstrong A, Ernande L, Flachskampf FA, Foster E, Goldstein SA, Kuznetsova T, et al. Recommendations for cardiac chamber quantification by echocardiography in adults: an update from the American Society of Echocardiography and the European Association of Cardiovascular Imaging. *J Am Soc Echocardiogr*. 2015;28(1):1–39.
- Rudski LG, Lai WW, Afilalo J, Hua L, Handschumacher MD, Chandrasekaran K, Solomon SD, Louie EK, Schiller NB. Guidelines for the echocardiographic assessment of the right heart in adults: a report from the American Society of Echocardiography endorsed by the European Association of Echocardiography, a registered branch of the European Society of Cardiology, and the Canadian Society of Echocardiography. *J Am Soc Echocardiogr*. 2010;23(7):685–713.
- Russell K, Eriksen M, Aaberge L, Wilhelmsen N, Skulstad H, Gjesdal O, Edvardsen T, Smiseth OA. Assessment of wasted myocardial work: a novel method to quantify energy loss due to uncoordinated left ventricular contractions. *Am J Physiol Heart Circ Physiol*. 2013;305(7):H996–1003.
- Russell K, Eriksen M, Aaberge L, Wilhelmsen N, Skulstad H, Remme EW, Haugaa KH, Opdahl A, Fjeld JG, Gjesdal O, et al. A novel clinical method for quantification of regional left ventricular pressure-strain loop area: a non-invasive index of myocardial work. *Eur Heart J*. 2012;33(6):724–33.
- Hubert A, Le Rolle V, Leclercq C, Galli E, Samsset E, Casset C, Mabo P, Hernandez A, Donal E. Estimation of myocardial work from pressure-strain loops analysis: an experimental evaluation. *Eur Heart J Cardiovasc Imaging*. 2018;19(12):1372–9.
- Previtero M, Azzolina D, Palermo C, Tenaglia RM, Sammarco G, Ruozi N, Aruta P, Illiceto S, Muraru D, Badano L. Role of non-invasive left ventricular pressure-strain loop to predict cardiac death and arrhythmic risk in patient with organic heart disease and reduced left ventricular ejection fraction. *J Am Coll Cardiol*. 2019;73(9):1625.
- Lustosa RP, van der Bijl P, El Mahdi M, Montero-Cabezas JM, Kostyukovich MV, Ajmone Marsan N, Bax JJ, Delgado V. Noninvasive myocardial work indices 3 months after ST-segment elevation myocardial infarction: prevalence and characteristics of patients with postinfarction cardiac remodeling. *J Am Soc Echocardiogr* 2020.
- Haugaa KH, Grenne BL, Eek CH, Ersbøll M, Valeur N, Svendsen JH, Florian A, Sjøli B, Brunvand H, Køber L, et al. Strain echocardiography improves risk prediction of ventricular arrhythmias after myocardial infarction. *JACC Cardiovasc Imaging*. 2013;6(8):841–50.
- Zhao H, Lee AP, Li Z, Qiao Z, Fan Y, An D, Xu J, Pu J, Shen X, Ge H, et al. Impact of intramyocardial hemorrhage and microvascular obstruction on cardiac mechanics in reperfusion injury: a speckle-tracking echocardiographic study. *J Am Soc Echocardiogr*. 2016;29(10):973–82.
- Hammoudi N, Watanabe S, Bikou O, Ceccaldi A, Fish K, Yamada KP, Miyashita S, Lebreton G, Hajjar RJ, Ishikawa K. Speckle-tracking echocardiographic strain analysis reliably estimates degree of acute LV unloading during mechanical LV support by impella. *J Cardiovasc Transl Res*. 2019;12(2):135–41.
- Hedwig F, Soltani S, Stein J, Schoenrath F, Potapov E, Knosalla C, Falk V, Knebel F, Knierim J. Global work index correlates with established prognostic parameters of heart failure. *Echocardiography (Mount Kisco, NY)*. 2020;37(3):412–20.
- Vonk-Noordegraaf A, Westerhof N. Describing right ventricular function. *Eur Respir J*. 2013;41(6):1419–23.
- Houard L, Benaets MB, de Meester de Ravenstein C, Rousseau MF, Ahn SA, Amzulescu MS, Roy C, Slimani A, Vancaeynest D, Pasquet A, et al. Additional prognostic value of 2D right ventricular speckle-tracking strain

- for prediction of survival in heart failure and reduced ejection fraction: a comparative study with cardiac magnetic resonance. *JACC Cardiovasc Imaging*. 2019;12(12):2373–85.
22. Lejeune S, Roy C, Ciocea V, Slimani A, de Meester C, Amzulescu M, Pasquet A, Vancraeynest D, Beauloye C, Vanoverschelde JL, et al. Right ventricular global longitudinal strain and outcomes in heart failure with preserved ejection fraction. *J Am Soc Echocardiogr*. 2020;33(8):973–984. e972.
 23. Perkins GD, Olasveengen TM, Maconochie I, Soar J, Wyllie J, Greif R, Lockey A, Semeraro F, Van de Voorde P, Lott C, et al. European resuscitation council guidelines for resuscitation: 2017 update. *Resuscitation*. 2018;123:43–50.
 24. Berglund E, Monroe RG, Schreiner GL. Myocardial oxygen consumption and coronary blood flow during potassium-induced cardiac arrest and during ventricular fibrillation. *Acta Physiol Scand*. 1957;41(2–3):261–8.
 25. Sandroni C, Cavallaro F, Antonelli M. Is there still a place for vasopressors in the treatment of cardiac arrest? *Crit Care*. 2012;16(2):213.
 26. Kapur NK, Reyelt L, Swain L, Esposito M, Qiao X, Annamalai S, Meyns B, Smalling R. Mechanical left ventricular unloading to reduce infarct size during acute myocardial infarction: insight from preclinical and clinical studies. *J Cardiovasc Transl Res*. 2019;12(2):87–94.
 27. Kapur NK, Paruchuri V, Urbano-Morales JA, Mackey EE, Daly GH, Qiao X, Pandian N, Perides G, Karas RH. Mechanically unloading the left ventricle before coronary reperfusion reduces left ventricular wall stress and myocardial infarct size. *Circulation*. 2013;128(4):328–36.
 28. Saku K, Kakino T, Arimura T, Sakamoto T, Nishikawa T, Sakamoto K, Ikeda M, Kishi T, Ide T, Sunagawa K. Total mechanical unloading minimizes metabolic demand of left ventricle and dramatically reduces infarct size in myocardial infarction. *PLoS ONE*. 2016;11(4):e0152911.
 29. Saku K, Kakino T, Arimura T, Sunagawa G, Nishikawa T, Sakamoto T, Kishi T, Tsutsui H, Sunagawa K. Left ventricular mechanical unloading by total support of impella in myocardial infarction reduces infarct size, preserves left ventricular function, and prevents subsequent heart failure in dogs. *Circ Heart Fail*. 2018;11(5):e004397.
 30. Suga H. Ventricular energetics. *Physiol Rev*. 1990;70(2):247–77.
 31. Suga H. Total mechanical energy of a ventricle model and cardiac oxygen consumption. *Am J Physiol*. 1979;236(3):H498–505.
 32. Burkhoff D, Mirsky I, Suga H. Assessment of systolic and diastolic ventricular properties via pressure-volume analysis: a guide for clinical, translational, and basic researchers. *Am J Physiol Heart Circ Physiol*. 2005;289(2):H501–512.
 33. Bonnet B, Jourdan F, du Cailar G, Fesler P. Noninvasive evaluation of left ventricular elastance according to pressure-volume curves modeling in arterial hypertension. *Am J Physiol Heart Circ Physiol*. 2017;313(2):H237–h243.
 34. Konstam MA, Abboud FM. Ejection fraction: misunderstood and over-rated (changing the paradigm in categorizing heart failure). *Circulation*. 2017;135(8):717–9.
 35. Mor-Avi V, Lang RM, Badano LP, Belohlavek M, Cardim NM, Derumeaux G, Galderisi M, Marwick T, Nagueh SF, Sengupta PP, et al. Current and evolving echocardiographic techniques for the quantitative evaluation of cardiac mechanics: ASE/EAE consensus statement on methodology and indications endorsed by the Japanese Society of Echocardiography. *Eur J Echocardiogr*. 2011;12(3):167–205.
 36. Galli E, Leclercq C, Hubert A, Bernard A, Smiseth OA, Mabo P, Samset E, Hernandez A, Donal E. Role of myocardial constructive work in the identification of responders to CRT. *Eur Heart J Cardiovasc Imaging*. 2018;19(9):1010–8.
 37. Cinotti R, Léopold V, Mebazaa A. A right insight in cardiogenic shock to get it right. *J Card Fail*. 2018;24(3):157–8.
 38. Schoenrath F, Hoch D, Maisano F, Starck CT, Seifert B, Wenger U, Ruschitzka F, Wilhelm MJ. Survival, quality of life and impact of right heart failure in patients with acute cardiogenic shock treated with ECMO. *Heart Lung*. 2016;45(5):409–15.
 39. Kapur NK, Langston P, Esposito ML, Burkhoff D. Abrupt development of a trans-aortic valve gradient in the setting of acute left-sided circulatory support identifies right heart failure in cardiogenic shock: The Kapur-Langston sign. *Cardiovasc Revasc Med* 2020.
 40. Mandawat A, Rao SV. Percutaneous mechanical circulatory support devices in cardiogenic shock. *Circ Cardiovasc Interv* 2017, **10**(5).
 41. Kapur NK, Esposito ML, Bader Y, Morine KJ, Kiernan MS, Pham DT, Burkhoff D. Mechanical circulatory support devices for acute right ventricular failure. *Circulation*. 2017;136(3):314–26.
 42. Zayat R, Ahmad U, Stoppe C, Khattab MA, Arab F, Moza A, Tewarie L, Goetzenich A, Autschbach R, Schnoering H. Sildenafil reduces the risk of thromboembolic events in heartmate ii patients with low-level hemolysis and significantly improves the pulmonary circulation. *Int Heart J*. 2018;59(6):1227–36.
 43. Ikonomidis I, Aboyans V, Blacher J, Brodmann M, Brutsaert DL, Chirinos JA, DeCarlo M, Delgado V, Lancellotti P, Lekakis J, et al. The role of ventricular-arterial coupling in cardiac disease and heart failure: assessment, clinical implications and therapeutic interventions. A consensus document of the European Society of Cardiology Working Group on Aorta & Peripheral Vascular Diseases, European Association of Cardiovascular Imaging, and Heart Failure Association. *Eur J Heart Failure*. 2019;21(4):402–24.
 44. Chantler PD, Lakatta EG, Najjar SS. Arterial-ventricular coupling: mechanistic insights into cardiovascular performance at rest and during exercise. *J Appl Physiol*. 2008;105(4):1342–51.

Publisher's Note

Springer Nature remains neutral with regard to jurisdictional claims in published maps and institutional affiliations.

Ready to submit your research? Choose BMC and benefit from:

- fast, convenient online submission
- thorough peer review by experienced researchers in your field
- rapid publication on acceptance
- support for research data, including large and complex data types
- gold Open Access which fosters wider collaboration and increased citations
- maximum visibility for your research: over 100M website views per year

At BMC, research is always in progress.

Learn more biomedcentral.com/submissions

